Advanced control methods for Asymmetrical Half-bridge Flyback

Alfredo Medina-Garcia, Francisco J. Romero, Diego P. Morales and Noel Rodriguez

***Abstract*— In this article, a power converter based on an asymmetrical half-bridge flyback topology is analyzed and optimized for small form factor and fast-charging power adaptors. Two resonant control methods, taking advantage of the forward and flyback characteristics of the converter, as well as the benefits of each of them depending of the operation point are discussed. The analysis is nourished with the equivalent circuits in each phase of operation and the equations that define them. Particularly innovative is the proposed zero voltage resonant valley switching (ZV-RVS) control method where the converter is operated similarly to a flyback converter and allows safe output voltage ramp up, which is one of the challenges that has limited the usage of this topology up to now. The manuscript also describes how to achieve high efficiency and power density using zero-voltage switching (ZVS) and zero-current switching (ZCS) techniques over the full range of the input voltage and the output load. Finally, the advantages of the proposed control methods are demonstrated in a 65 W adaptor prototype achieving a peak efficiency over 94.6% and an efficiency of 93.8% @ Vac ≥ 100V at full load over the range of the input voltage, as well as a world-class power density of 35 W/inch^3 uncased.**

***Index Terms*—Adaptor, efficiency, flyback, MOSFET, power density**

I. Introduction

Portable electronic devices offer every day more processing capabilities, new features and longer battery lifetime. Additionally, bigger screen sizes are becoming popular. All these features require batteries with higher energy capacity. Under such scenario, fast charging technologies are being developed to compensate the longer charging time required; those include new batteries, charging modes, and communication protocols between charger and the portable device to provide variable output voltage, ie. quick charge, USB-PD [1], etc. These standards allow, as well, the reuse of the power adaptors for different devices and ensure minimal waste of electronics [2] but rise an additional challenge when they are compared to fix voltage adaptors.

One key feature to enable fast charging is that the adaptor must be able to provide a higher power level, however its size and weight increase with the amount of power that the charger can provide. This increase of size and weight is contradictory with the portability offered by the devices themselves. This contradiction is driving the search for new solutions that are able to keep the adaptor size reasonable but to increase the amount of power that it can provide; this kind of solutions are known as high power density adaptors.

The potential of reducing the adaptor size is limited not only by the size of the individual components, but as well by the maximum losses that are generated at any given operating point. In contrast to other solutions, the heat of adaptors for portable applications is only dissipated by the case surface with passive cooling. The maximum surface temperature is usually determined by the minimum efficiency at full load [3]. Typically this occurs at the minimum input voltage: 100Vac for universal input range 100Vac to 240Vac.

The flyback topology, and its derivatives, is one of the most suitable topologies to overcome the wide input to output voltage range; it is the dominating topology for adaptors below 75W where no power factor correction (PFC) is required [4]. In a traditional flyback converter [5], the transformer acts as a pure energy storage element resulting in a larger transformer size when it is compared to forward topologies [6]. This limits the maximum achievable power density. In recent years, the emerging wide bandgap devices, such as GaN or SiC [7]-[9], allow higher operation frequencies. This has enabled the active clamp flyback (ACF), in its complementary and non-complementary versions [10]-[13], in combination with these new devices, to reduce the transformer size by increasing the frequency since it is able to recycle the energy of the parasitic elements. Nevertheless, the higher switching frequencies are not exempt from problems. The frequency increase is linked to the usage of wide band gap devices. Faster switching frequencies raise new challenges, i.e. fulfilling conductive or radiated electromagnetic interference (EMI) regulations, such as EN55022 [14].

The asymmetrical hybrid flyback has been proposed by several papers [15]-[18] as a topology able to boost efficiency by recycling the energy of the parasitic elements and, reduce the transformer size due to its hybrid properties as flyback and forward converter. However, the proposed control methods do not address the challenges that arise during power up, due to wide output voltages or lower efficiency at low output currents.

Alfredo Medina-Garcia Author, Infineon Technologies AG, Neubiberg, 85570, Germany (e-mail: alfredo.medina-garcia@infineon.com).

Francisco J. Romero, Diego P. Morales and Noel Rodriguez, Department of Electronics and Computer Technology at the University of Granada 18071 Granada, Spain (emails: franromero@ugr.es, diegopm@ugr.es; noel@ugr.es).

In this paper, a detailed analysis of the asymmetrical half-bridge (AHB) flyback and its equations will be performed, two control methods will be proposed to overcome the challenges that arise from high power density and wide output voltage. Furthermore, the control methods introduced will ensure optimum usage of the topology in all operation points.

II. Topology

The general schematic of the asymmetrical half-bridge flyback converter is presented in Fig. 1, including the elements needed in an adaptor, such as the EMI filter and the input rectifier. The circuit shows a half-bridge in the primary side connected to a capacitor (C_r) in series with the transformer. This is similar to an LLC converter [19], showing the resonant nature of the converter. On the other hand, the secondary side, with a single diode, is similar to a flyback converter.

Of particular interest is the auxiliary winding L_{aux}, that will provide additional information used in the proposed control methods. This winding will be used to detect when the magnetizing current reaches zero through the connection to the controller input ZCD (zero crossing detection).

Aiming to provide outstanding power density, the control methods for this topology have been developed to achieve ZVS and secondary ZCS under all conditions of input voltages and output current. Moreover, this topology recycles the energy of

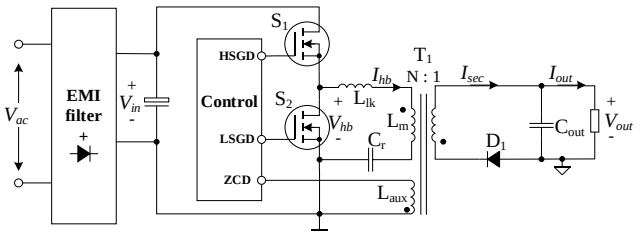

Fig. 1. Simplified typical adaptor schematic with AHB flyback stage.

the transformer leakage inductance, which helps to reduce the losses and maximize efficiency. To further boost efficiency, synchronous rectification can be used in the secondary side [20]. It is worth mentioning that the converter can also be implemented by connecting the resonant capacitor Cr and the primary side of the power transformer between the positive node V_{in} and the middle point of the half-bridge. This would result in a similar operation, but with the roles of the switch S1 and S2 exchanged.

III. Continuous Resonant Mode (CRM) Operation

Continuous Resonant Mode (CRM) is a control method consisting in turning on the switches in a complementary way with dead times in between to avoid cross conduction. In this mode, there is always a voltage applied to the primary winding of the transformer, except for small dead times.

The ON time of the high side switch S1, Fig. 1, can be time controlled [21] or peak current controlled [22]. Peak current control is more suitable as it ensures that the output current can be limited and undesired effects such as body diode cross conduction can be avoided [23]-[25].

A. Equations

An example of CRM mode waveforms in steady state, obtained by computer numerical method, is shown in Fig. 2. The numerical solution accounts for a value of typical switches ON resistance (R_{on}) of 0.2 Ω, and 65W output power. The rest of components values are: L_m = 51.5µH (primary magnetizing inductance of the transformer), L_{lk} = 1.5µH (leakage inductance of the transformer referred to primary), N = 2.8, C_r = 300nF, V_{in} = 130V, V_{out} = 20V.

In such case, three different phases of operation are identified corresponding to the time intervals, t_0-t_1 (phase 1), t_1-t_2 (phase 2) and t_2-t_3 (phase 3). Depending on the conditions, phases 2 and 3 may change the order or appear more than one time; these situations will be discussed later in section III.B.

Looking at the different phases of operation of the converter, equivalent circuits can be used to represent each of them with its respective equations which define the operation. For a pure theoretical study, ideal components with no parasitic elements will be considered and dead times in the half-bridge are assumed to be zero.

The 3 phases shown in Fig. 2 can be named according to the effect that they have in the converter as charge, transfer and

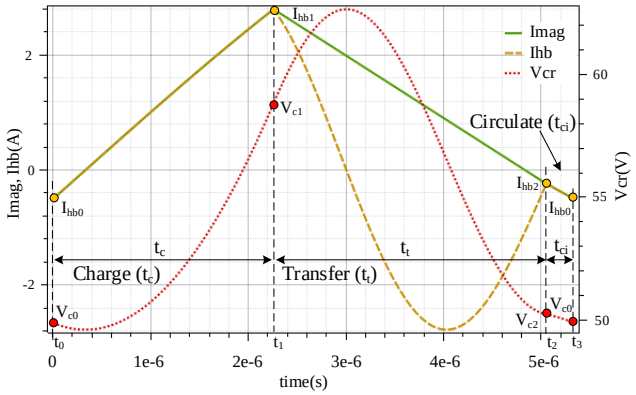

Fig. 2. Hybrid flyback CRM steady state waveforms (conditions L_m = 51.5µH, L_{lk} = 1.5µH, N = 2.8, C_r = 300nF, V_{in} = 130V, V_{out} = 20V, I_{out} = 3.25A).

circulate phase. In the following paragraphs, the equivalent circuit and equations are presented:

Phase 1, *charge*, from t_0 to t_1: High side switch ON, low side switch OFF.

The equivalent circuit is shown in Fig. 3. In this phase, the input voltage is connected to the LC tank formed by the primary inductance (L_p, $L_p = L_{lk} + L_m$) and the resonant capacitor (C_r). The resulting LC tank will be underdamped as no resistive elements are considered. On a practical case the circuit is normally underdamped since the ON series resistance of the switch (R_{on}) and other elements such as transformer winding resistance, PCB tracks, etc are typically very low.

With the previously described considerations, the equations that define the current in the loop and the voltage of the resonant capacitor are given by (1) and (2).

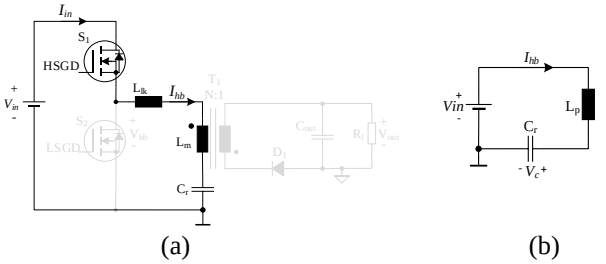

Fig. 3. Phase 1, charge: (a) Active elements (b) Equivalent circuit.

$$i_{hb}(t) = I_{hb0}\cos(w_p t) + \frac{V_{in}-V_{c0}}{Z_p}\sin(w_p t) \quad (1)$$

$$v_c(t) = (V_{c0}-V_{in})\cos(w_p t) + I_{hb0}Z_p \sin(w_p t) + V_{in} \quad (2)$$

Being $w_p = 1/\sqrt{L_p C_r}$ and $Z_p = \sqrt{L_p/C_r}$, I_{hbo} represents I_{hb} at $t = t_0$.

Phase 2, *transfer*, from t_1 to t_2: High side switch OFF, low side switch ON and $I_{mag} \neq I_{hb}$. (Being I_{mag} the current that represents the magnetizing current of the transformer)

During this phase, the equivalent circuit is shown in Fig. 4. C_{out} is considered large enough to assume that the voltage across it during once cycle is constant; this allows to represent it as a voltage source of value NV_{out} in the primary side equivalent circuit. During this phase of operation, three reactive elements which energy is changing, L_m, L_{lk} and C_r, are dominating the characteristics of the circuit:

1) The energy of the magnetizing inductance L_m is absorbed by the output capacitor, in this case represented by NV_{out}.
2) The LC tank formed by L_{lk} and C_r is left free to oscillate and their energy flows to the output capacitor too.

The addition of the current from both tanks defines the output current I_{sec}. The reflected secondary side current (to primary side) can defined as $I_{sec\_p} = I_{sec} / N$.

The equations describing the electrical magnitudes in this phase are given by (3) to (6):

$$i_{hb}(t) = I_{hb1}\cos(w_l t) + \frac{NV_{out}-V_{c1}}{Z_l}\sin(w_l t) \quad (3)$$

$$v_c(t) = (V_{c1}-NV_{out})\cos(w_l t) + I_{hb1}Z_l \sin(w_l t) + NV_{out} \quad (4)$$

$$i_{lm}(t) = I_{hb1} - \frac{NV_{out}}{L_m}t \quad (5)$$

$$i_{sec\_p}(t) = i_{mag}(t) - i_{hb}(t) \quad (6)$$

Where $w_l = 1/\sqrt{L_{lk}C_r}$ and $Z_l = \sqrt{L_{lk}/C_r}$. I_{hb1} represents I_{hb} at $t = t_1$.

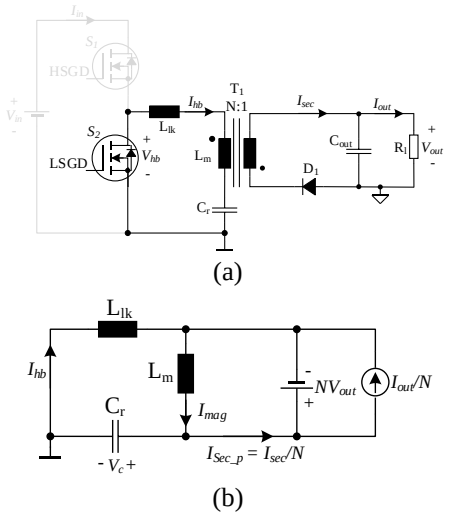

Fig. 4. Phase 2, transfer: (a) Active elements (b) Equivalent circuit.

Phase 3, *circulate*, from t_2 to t_3: High side switch OFF, low side switch ON and $I_{mag} = I_{hb}$.

This phase starts when I_{hb} current is equal to I_{mag}, meaning that I_{sec} reaches and stay at 0A since the output diode blocks the current. In this phase, the low side switch is kept ON ensuring that I_{hb} gets negative. The negative current in L_p, allows having ZVS at the next turn on of the high side switch. If devices with body diode are used, i.e. MOSFET, special care needs to be taken in order to ensure that I_{hb} is negative when the high side switch turns ON in the next cycle. Otherwise an undesired effect called body diode cross conduction will result into a high spike of current through the half-bridge due to the body diode turn off delay of the low side switch [24].

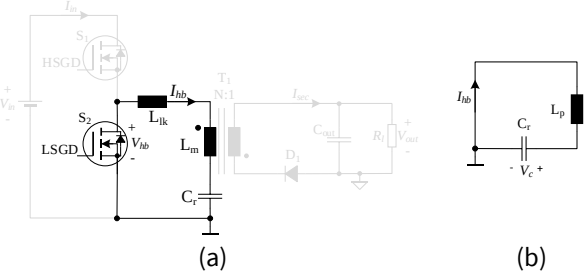

Fig. 5. Phase 3. Circulate: (a) Active elements (b) Equivalent circuit.

The equations defining this phase are (7) and (8).

$$i_{hb}(t) = I_{hb2}\cos(w_p t) + \frac{V_{c2}}{Z_p}\sin(w_p t) \quad (7)$$

$$v_c(t) = V_{c2}\cos(w_p t) + I_{hb2}Z_p \sin(w_p t) \quad (8)$$

Considering a steady state the following system of equations can be derived:

$$I_{hb1} = I_{hb0}\cos(w_p t_c) + \frac{V_{in}-V_{c0}}{Z_p}\sin(w_p t_c) \quad (9)$$

$$V_{c1} = (V_{c0}\text{-}V_{in})\cos(w_p t_c) + I_{hb0} Z_p \sin(w_p t_c) + V_{in} \quad (10)$$

$$I_{hb2} = I_{hb1}\cos(w_l t_t) + \frac{NV_{out}\text{-}V_{c1}}{Z_l}\sin(w_l t_t) \quad (11)$$

$$V_{c2} = (V_{c1}\text{-}NV_{out})\cos(w_l t_t) + I_{hb1} Z_l \sin(w_l t_t) + NV_{out} \quad (12)$$

$$I_{hb2} = I_{hb1}\text{-}\frac{NV_{out}}{L_m} t_t \quad (13)$$

Where

$$I_{hb0} = I_{hb2}\cos(w_p t_f) + \frac{V_{c2}}{Z_p}\sin(w_p t_f) \quad (14)$$

$$V_{c0} = V_{c2}\cos(w_p t_f) + I_{hb2} Z_p \sin(w_p t_f) \quad (15)$$

And I_{hb2} represents I_{hb} at $t = t_2$.

B. *Low output current operation*

As the output current decreases, the order and number of the previously shown phases change. Fig. 6 shows the waveforms of the previous circuit example under 1A of load and 20V output.

A lower output current leads to a higher negative I_{hb} current, therefore the voltage in the resonant capacitor at the end of the charge phase has a value lower than the reflected output voltage NV_{out}, this leads, during the low side switch turn on, to a circulating phase followed by transfer and circulating phase again. In the case of no load condition, the magnetizing average current would be zero and the half-bridge would just drive an LC circuit circulating energy. Consequently, at low output current, the resulting efficiency of the converter using this control method is expected to be low due to the amount of circulating energy compared to the energy transferred to the secondary side.

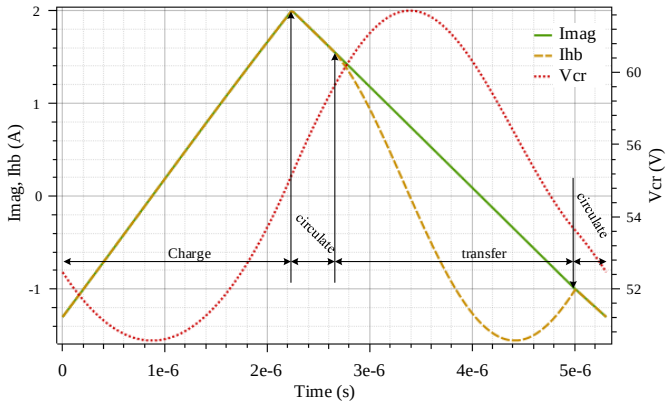

Fig. 6. CRM steady state waveforms under 1A output current and 20V (L_p = 53µH, L_{lk} = 1.5µH, N = 2.8, C_r = 300nF, V_{in} = 130V and V_{out} = 20V).

C. *Low output voltage operation*

In CRM mode, lower output voltages can be provided by decreasing the duty cycle defined as $T_{hs}/(T_{hs} + T_{ls})$, where T_{hs} and T_{ls} are the ON times of the high side and low side switches respectively. Under these conditions, the resonance seen during the energy transfer phase may not match the ON time of the low side switch T_{ls}. In this case, where T_{ls} is longer comparable to previous examples, several resonant cycles of the LC tank formed by L_{lk} and C_r may occur; this is illustrated in Fig. 7.

Another important aspect to consider is the synchronous rectification in the secondary side [20], present in almost every modern high-density adaptor to increase the efficiency. In CRM mode, the shape of the secondary current (I_{sec_p}), during T_{ls}, may vary depending on the damping factor due to the equivalent series electrical resistance of the circuit as shown in Fig. 7. The equivalent series resistance R_{esr} includes the effect of the switches ON resistance (R_{on}), pcb tracks, transformer cables, etc. Fig. 7 shows two examples for different R_{on} values, in Fig. 7(a) R_{on} = 0.2 Ω and Fig. 7(b) R_{on} = 1 Ω.

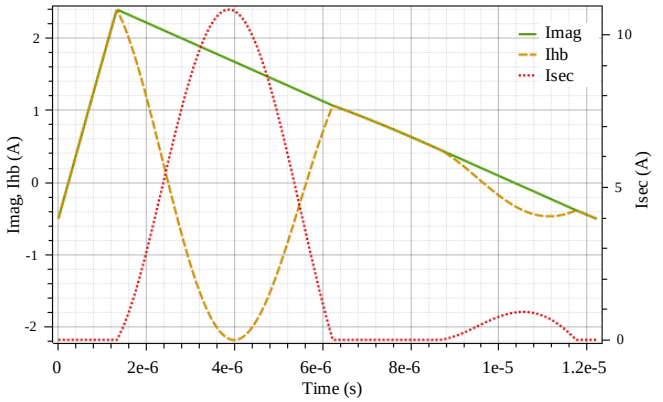

(a)

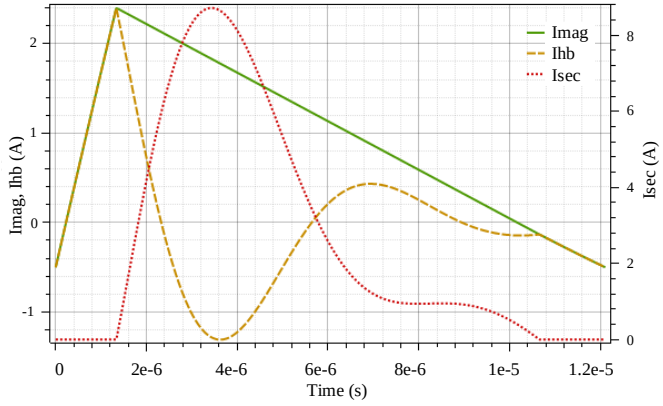

(b)

Fig. 7. Damping effect on the waveforms shape for low output voltage (V_{out} = 5V). a) I_{sec_p} with 2 pulses, series resistance R_{esr}: 0.2 Ω, b) I_{sec_p} with single pulse, series resistance R_{esr}: 1 Ω

In Fig. 7(a) the output current reaches zero amperes and rises again; typically, SR controllers activate the associated switch only during the first pulse and not during the second, affecting this way the efficiency. If synchronous rectification is used in combination with CRM control method for low output voltage, the operation in Fig. 7(b) is preferred, due to single current pulse in the secondary.

D. *Low input voltage operation*

During low input voltage operation, the required T_{hs} to reach

certain amount of peak current is longer. The current I_{hb}, which has a sinusoidal shape (1), may reach its maximum and start decreasing during the charge phase, meaning that peak current control cannot be used since I_{hb} may not reach the desired peak value; ON time control may be used in this case or combined with peak current control. Under these conditions, I_{hb}, during the charge phase, cannot be approximated by a lineal function, therefore, the approximations presented in [23] are no longer

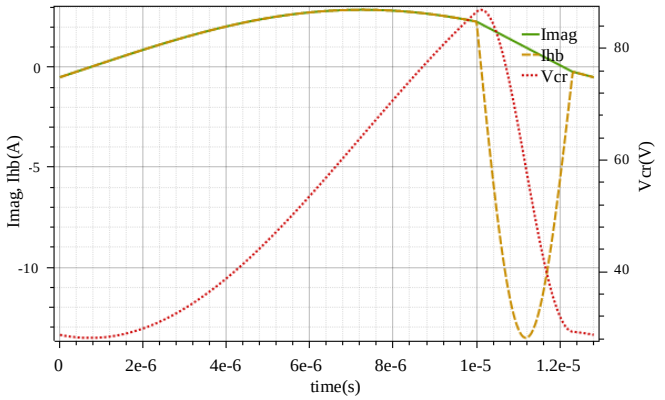

Fig. 8. Sinusoidal shaped current I_{hb} during charge time at low input voltage (V_{in} = 63V).

valid. This operation condition is shown in Fig. 8. As the current I_{hb} decreases, the energy stored in the magnetizing inductance of the transformer decreases, besides this, the energy stored in the capacitor increases further. This differs from the energy portion shared between the resonant capacitor and the magnetizing inductance presented in [23] under lineal approximation of the current I_{hb}. In this situation, much more energy is stored in the resonant capacitor compared to the energy stored in the magnetizing inductance.

To understand further the behavior of the converter, the system of equations presented by (9) to (15) needs to be solved. Since the transfer time variable t_t appears in (13) and, as well, within the argument of a trigonometrical functions in (11) and (12), the system is transcendental and cannot be solved symbolically. To disclose the limits of the converter at low input voltage, where the lineal approximations of I_{hb} are no longer valid, the same numerical iterative method mentioned in section III.A will be used.

The numerical solution will consider practical conditions required for a proper operation:

1) At the end of the cycle (t_3 in Fig. 2) $I_{hb} = I_{mag}$ to have secondary ZCS
2) At the end of the cycle I_{mag} needs to be negative to achieve ZVS
3) V_{out} is constant and the amplitude I_{mag} (peak to peak value) is kept constant

The solution is presented in Fig. 9, it shows the relation between the output current (y axis) and input voltage (x axis) for different values of I_{hb_peak} (parameter). It can be observed that a given I_{hb_peak} current allows higher output current at lower V_{in}. The left part of the plot (lower values of the input voltage), where the lines start to curve up, shows the limit of the lineal

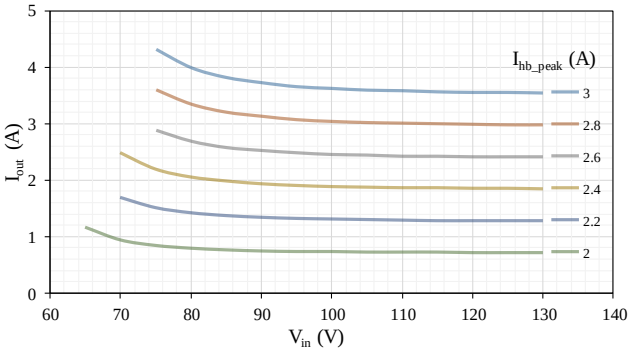

Fig. 9. I_{out} as a function of V_{in} for different I_{hb} peak currents showing the limits of lineal approximation for I_{hb}

approximation of the sinusoidal shaped current I_{hb} described in [23]. Nevertheless, from a practical point of view, the approximation is accurate down to relatively low input voltages.

For dimensioning of a practical converter, it is desired to know the value of the minimum operating input voltage. Such voltage can be chosen as the minimum one to ensure peak current control of I_{hb}, meaning that I_{hb} does not have negative slope. That is the peak of the sine wave during the charge phase. This is shown in Fig. 10.

Considering the results shown in Fig. 9, a conservative approximation of the required I_{hb} peak current can be calculated using (20) as proposed in [23].

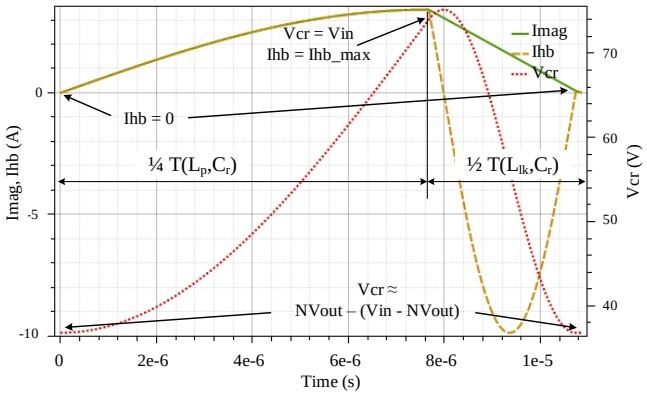

Fig. 10. Converter waveforms showing the limit of peak current (I_{hb}) control.

With a few practical approximations, we can calculate the minimum input voltage required to reach the desired I_{hb} peak:

1) Assuming zero magnetizing negative current, we can reduce (1) to (16) and the peak of I_{hb} to (17).

$$i_{hb}(t)=\frac{V_{in}-V_{c0}}{Z_p}\sin(w_p t) \tag{16}$$

$$I_{hb\_max}=\frac{V_{in}-V_{c0}}{Z_p} \tag{17}$$

2) If the transfer phase (see section III.A) duration is approximately equal to half-resonant period of the tank formed by L_{lk} and C_r, the initial voltage in the

resonant capacitor can by calculated by (18).

$$V_{c0} = NV_{out}-(V_{in}-NV_{out}) \quad (18)$$

$$V_{in\_min} = NV_{out}+\left(\frac{I_{out}}{N}\right)\sqrt{L_p/C_r} \quad (19)$$

Replacing the required peak current I_{hb_max} from (20) and V_{c0} from (18) in (17), we obtain the approximate minimum input voltage required for peak current control (19).

E. Limitations of the CRM control method.

CRM (continuous resonant mode) control method provides the best efficiency at high output current; however, at low output current, the excessive circulating current impacts negatively on the efficiency. Furthermore, at low output voltage, double pulse in the secondary current, as seen in Fig. 7(a), may be observed, leading to loss of ZCS in the secondary and undesired ringing. Additionally, if a synchronous rectifier (SR) is used, a loss of efficiency may occur since the SR controller may only be triggered during the first pulse of the secondary current.

However, the most challenging drawback from a practical point of view is that the current I_{hb} may not reach a negative value at the end of the cycle (t_3 in Fig. 2), especially during ramp up of the output voltage from zero. If MOSFETs are used as switches, there is risk of body diode cross conduction [24]-[25].

To overcome those limitations, an alternative control method will be proposed, this control method will be presented in the next section.

IV. ZERO VOLTAGE RESONANT VALLEY SWITCHING (ZV-RVS) MODE

Zero Voltage Resonant Valley Switching mode is a control method that operates the converter using waiting times (both switches OFF) until the transformer is demagnetized. It is synchronized to the valleys as a traditional quasi-resonant flyback [5], which allows the converter to reduce the frequency and it ensures zero voltage switching in all switches. This mode solves the weakness of the previously analyzed CRM control method, especially during start up with low output voltage since it ensures no body diode cross conduction and keeps the magnetizing current under control.

Fig. 11 shows the result of a simulation of the proposed control method ZV-RVS. The PWM pattern is shown in the upper part of the figure, where HS and LS signals indicate which switch is active over time. The PWM consists of three pulses synchronized with the zero crossing detection (ZCD) signal, see Fig. 1, which indicates the demagnetization of the transformer and subsequent zero crossing of the magnetizing current. This signal is commonly used in quasi-resonant flyback converters [5].

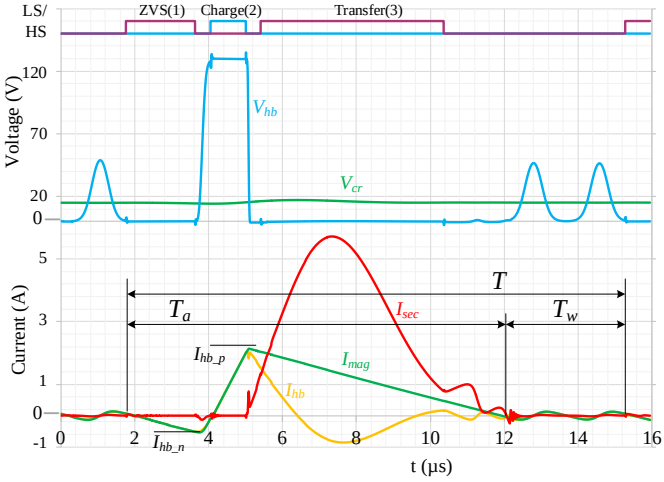

Fig. 11. Simulated ZV-RVS waveforms with 2nd valley operation. T_a is the period with forced magnetizing current and T_w is the period of free oscillation.

The function of the three pulses and the waiting time is the following:

1) ZVS pulse (1): it is applied on the low side (LS) switch when V_{hb} reaches zero (detected through the ZCD signal). This pulse is used to induce a small amount of I_{hb} negative current in the transformer. After the LS turns off the induced current forces V_{hb} to increase, allowing ZVS for the next pulse.
2) *Charge* pulse (2): this pulse is applied on the high side (HS) switch. During this pulse the current I_{hb} gets positive and the energy taken from the input is stored in the primary inductance and the resonant capacitor.
3) *Transfer* pulse (3): This last pulse, in the low side switch, will transfer the stored energy to the secondary side, the energy of the resonant capacitor is transferred in forward mode through the transformer. Once this pulse is finished the remaining magnetizing current, if any, will be transferred to the output or the resonant capacitor.
4) Waiting time (T_w): during this time the remaining energy in the magnetizing inductance flows to the output capacitor (and/or the resonant capacitor); the transformer magnetizing inductance is discharged and the system oscillates freely.

Special attention needs to be paid to the transfer pulse. In the proposed ZV-RVS mode, the transfer pulse should be shorter than the demagnetization time of the transformer to allow free oscillations once the magnetizing current reaches zero. These oscillations are similar to those occurring in standard flyback converters [5]. The next *ZVS* pulse can be synchronized to any valley controlling this way the switching frequency [26].

It is worth mentioning that this control method outperforms other alternatives since it ensures no body diode cross conduction, allows frequency control, zero voltage switching in all cases, uses forward mode energy transfer, and it maximizes the efficiency, due to the absence of extra circulating energy,

compared to CRM mode.

A. ZV-RVS mode, output current and control.

The output current in CRM mode under lineal approximation of I_{hb} is similar to the one of a buck converter operating in CCM mode:

$$I_{out} = \frac{N\left(I_{hb\_p}+I_{hb\_n}\right)}{2} \tag{20}$$

This is analyzed in detail in [23]. Having a look to the waveforms shown in Fig. 11 for ZV-RVS mode it can be observed that, without considering the pause interval T_w, the magnetizing current, I_{hb}, has the same triangular shape as it has for CRM mode. Therefore, we can approximate the output current taking into account the duty cycle (T_a/T) shown in (21).

$$I_{out} = \frac{N\left(I_{hb\_p}+I_{hb\_n}\right)}{2}\frac{T_a}{T} \tag{21}$$

Similar to a standard flyback, with this method, we have two degrees of freedom to control the output current, namely I_{mag} peak current and valley number selection (or waiting time). The valley number will introduce a waiting time where no power is transferred. This method allows reducing circulating current present in CRM control method, achieving in this way a higher efficiency at low output current.

V. Practical Prototype

To demonstrate the high efficiency and power density that this topology can achieve, a 65W prototype converter was built. The converter specifications are shown in Table 1.

TABLE 1
CONVERTER SPECIFICATIONS

Parameter	Value
Output voltage	USB-PD 5V-20V
Nominal output current	3.25A
Input voltage	90Vac – 264Vac
Power density uncased	35 w/inch^3
Efficiency full load	>93.8% @ Vac ≥ 100Vac
EMC	EN55022 class B

The dimensioning of the converter [27] has targeted maximizing the efficiency at low input voltage and maximum load, this helps minimizing the maximum power loss at any given operation point. A synchronous rectifier was used in the secondary side in order to further boost the efficiency. The MOSFETs used in the experimental prototype and their characteristics are shown in Table 2. To reduce the circulating current I_{hb} required to achieve ZVS and maximize efficiency, the primary side switches were selected with a low output capacitance C_{oss} and low $R_{ds(on)}$. Since the half-bridge transistor's body diodes clamp the voltage in the bridge middle point V_{hb}, the maximum V_{ds} voltage rating required by the primary MOSFETS is limited to the AC wave peak voltage. This is a major advantage compared to a standard flyback converter or active clamp flyback (ACF) converter where additional reflected voltage and spikes need to be consider. This lower voltage seen across the transformer primary and secondary is another advantage for EMI and primary to secondary safety distances compared to ACF.

TABLE 2
MOSFET USED IN THE CONVERTER

Parameter	LS Mosfet	HS Mosfet	SR Mosfet
Company	Infineon	Infineon	Infineon
Reference	IPI50R140CP	IPD60R180C7	BSC093N15S5
$R_{ds(on)}$	140 mΩ	180 mΩ	9.3 mΩ
V_{ds_max}	500 V	600 V	150V
$C_{o(tr)}$	230 pF	349 pF	604 pF
Q_{gs}	48 nC	24 nC	14 nC

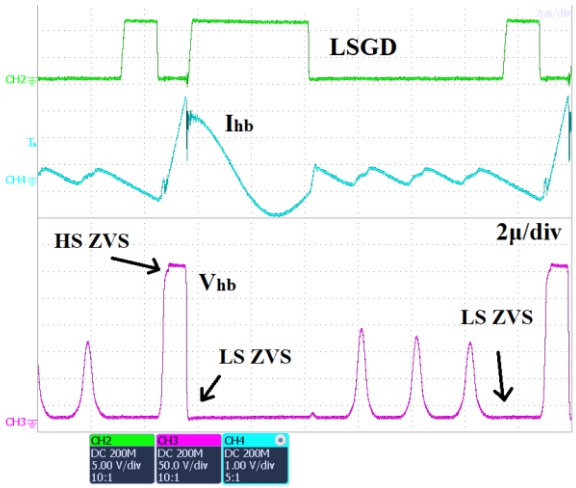

Fig. 12. Actual waveforms of the converter prototype during ZV-RVS operation Measured with scope DLM6054. Operations conditions: V_{ac} = 230V, V_{out} = 12V.

The transformer was implemented using an RM8 core for size reduction. The specifications are shown in Table 3.

TABLE 3
TRANSFORMER SPECIFICATIONS

Parameter	LS Mosfet
Core type	RM8
Core material	PC95
L_m	52µH
L_{lk}	1.7µH
N_p	17 turns (Litz 40x0.1 mm)
N_s	6 turns (TIW Litz 120x0.08 mm)
Winding structure	P-S-P

Both discussed control methods, CRM and ZV-RVS, were implemented in a programmable digital controller from Infineon Technologies AG.

Fig. 14 shows the converter efficiency for the two control modes versus output current, for 100Vac and 240Vac.

It can be observed, as explained, that RVS is preferred for low output current and CRM mode for higher output currents. Using both modes, the total efficiency can be optimized.

An actual waveform of the RVS mode is shown in Fig. 12.

The EMI results at 115Vac and 230Vac are shown in Fig. 13. They fulfill the required normative EN55022 [14] for average and quasi peak limits.

It can be seen how the proposed method achieve ZVS, or in worst case partial ZVS, for both switches as explained in

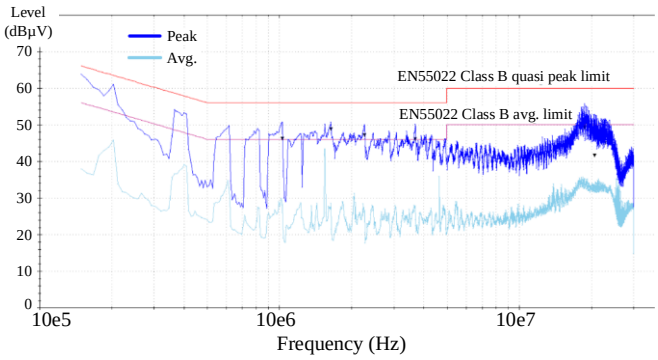

(a)

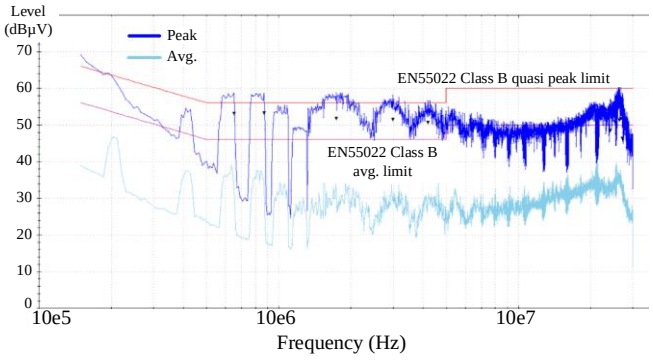

(b)

Fig. 13. Conductive EMI results, average and peak values. a) V_{ac} = 115 V, full load and b) V_{ac} = 230 V, full load.

section IV. After the transfer pulse, V_{hb} oscillates similarly to a standard flyback converter. This operation mode solves the issue of the high circulating current that leads to low efficiency

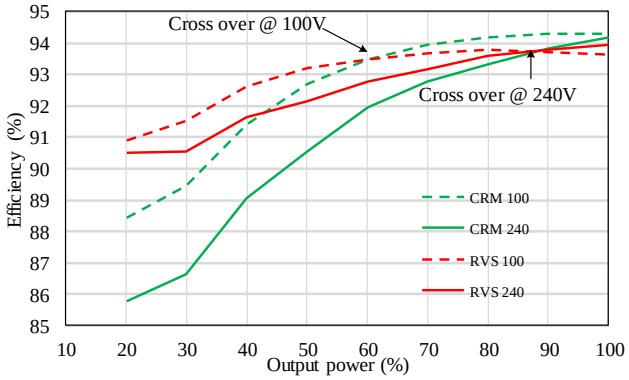

Fig. 14. Converter efficiency vs. load at 100Vac and 240Vac input voltage using CRM and RVS mode. Output voltage 20V.

at low output current seen in Fig. 14.

The size of the final converter, see Fig. 15(a), is 43.3 × 37 × 19 mm, achieving an uncased power density of 2.13W/cm^3 (35 W/inch^3). The prototype achieved a minimum efficiency of 93.1% at a 90Vac/50Hz input and a 65 W load measured at the board connectors.

The frequency of operation ranged from approximately 140 KHz at 90 Vac to 240 KHz at 264 Vac.

(a)

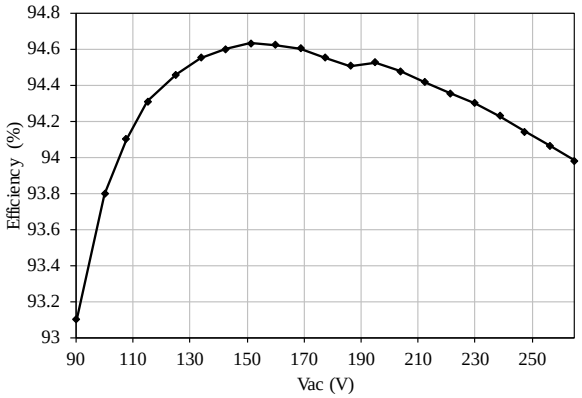

(b)

Fig. 15. (a) Asymmetric HB flyback prototype; (b) full load efficiency versus input voltage range.

VI. Conclusions

In the previous sections, two different control methods have been developed and presented for AHB flyback converter. It is important to sum up the nature of both control methods:

1) CRM is a typical operation mode of forward converters, i.e. a buck converter. The duty cycle defines the output voltage. In CRM mode, the converter can operate in absence of load without losing the control of the output voltage, meaning that energy is just circulated but not transferred.
2) In ZV-RVS mode, the converter is operated similar to a flyback converter. The PWM used in this control method guarantees always zero voltage switching (ZVS) and minimizes the circulating energy. It can also perform valley switching, reducing this way the switching frequency to improve the efficiency.

The dual control mode proposed in this work, makes the best use of the converter due to its hybrid nature forward/flyback in terms of wide input/output voltage range, low output current operation and maximum efficiency. Additionally, it ensures that

the output current and/or voltage are easy to control. The selected topology in combination with the two described control methods enables high power density (35W/inch^3) and high full load efficiency, above 93.1% over input voltage, using Silicon MOSFETs as switches. Additionally, the newly proposed ZV-RVS mode solves the weakness of the CRM mode for low output current, low output voltage and converter start up. It ensures the demagnetization of the transformer and avoids body diode cross conduction issues and therefore safe start-up. The results have been demonstrated with a fully functional 65W prototype.

ACKNOWLEDGMENT

The authors would like to thank Dr. Manfred Schlenk and Mr. Sandro Cerato for their support and help.

Infineon Technologies AG has sponsored this work.

REFERENCES

[1] www.usb.org. Universal Serial Bus Power Delivery Specification, version 2.0, revision 3.0, 07.Feb.2020.

[2] Victor Toral-Lopez, Cristian Gonzalez, Francisco J. Romero Maldonado, Encarnacion Castillo, Luis Parrilla, Antonio Garcia, Noel Rodriguez, Almudena Rivadeneyra, Diego P. Morales, "Reconfigurable Electronics: addressing the uncontrolled increase of Waste Electrical and Electronic Equipment" *Resources, Conservation & Recycling* Q1, Volume 138, November 2018, Pages 47-48.

[3] Manfred Schlenk: Alfredo Medina-Garcia; Christian Wald. "High-Power-Density Adapters and Chargers – Challenges and Solutions" *Bodo's power system*, ISSN: 1863-5598, November 2019, pp. 42-45.

[4] IEC Electromagnetic compatibility (EMC) - Part 3-2: Limits - Limits for harmonic current emissions (equipment input current <= 16 A per phase), *International Electrotechnical Commision*, IEC 61000-3-2:2014.

[5] H. Onay, -. Volkan Sueel and A. Hava, "A Comprehensive Loss Analysis of Quasi Resonant Flyback Converter for Design Purpose," *PCIM Asia 2018; International Exhibition and Conference for Power Electronics, Intelligent Motion, Renewable Energy and Energy Management*, Shanghai, China, 2018, pp. 1-8.

[6] L. M. Redondo and J. F. Silva, "Flyback Versus Forward Switching Power Supply Topologies For Unipolar Pulsed-Power Applications," *IEEE Transactions on Plasma Science*, vol. 37, no. 1, pp. 171-178, Jan. 2009, doi: 10.1109/TPS.2008.2006056.

[7] Deboy, G., Kasper, M.J., Medina-Garcia, A., Schlenk M. "A New Era in Power Electronics with Gallium Nitride," *ETG Journal*, 2nd edition, 2018, pp. 6-11.

[8] V. Pala *et al*., "900V silicon carbide MOSFETs for breakthrough power supply design," *2015 IEEE Energy Conversion Congress and Exposition (ECCE)*, Montreal, QC, 2015, pp. 4145-4150, doi: 10.1109/ECCE.2015.7310245.

[9] L. Garcia-Rodriguez, E. Williams, J. C. Balda, J. Gonzalez-Llorente, E. Lindstrom and A. Oliva, "Dual-stage microinverter design with a GaN-based interleaved flyback converter stage," *2013 IEEE Energy Conversion Congress and Exposition*, Denver, CO, 2013, pp. 4496-4502, doi: 10.1109/ECCE.2013.6647302.

[10] Xue, L.; Zhang, J. "Active clamp flyback using GaN power IC for power adapter applications" in *Proc. IEEE Applied Power Electronics Conference and Exposition (APEC)*, Tampa, FL, USA, 26–30 March 2017; pp. 2441–2448.

[11] Alou, P.; Garcia, O.; Cobos, J.A.; Uceda, J.; Rascon, M. "Flyback with active clamp: A suitable topology for low power and very wide input voltage range applications" in *Proc. IEEE Applied Power Electronics Conference and Exposition (APEC)*, Dallas, TX, USA, 10–14 March 2002; pp. 242–248, doi:10.1109/APEC.2002.989254.

[12] Watson, R.; Lee, F.C.; Hua, G.C. "Utilization of an active-clamp circuit to achieve soft switching in flyback converters," *IEEE Transactions on Power Electronics*, vol. 11, no. 1, Jan. 1996, pp. 162–169, doi:10.1109/63.484429.

[13] A. Bianco, C. Adragna, S. Saggini, M. Ursino, F. Ciappa and G. Scappatura, "A Novel Noncomplementary Active Clamp Flyback Control Technique," 2019 *IEEE Applied Power Electronics Conference and Exposition (APEC)*, Anaheim, CA, USA, 2019, pp. 2155-2158, doi: 10.1109/APEC.2019.8721838.

[14] EN Information technology equipment - Radio disturbance characteristics - Limits and methods of measurement, EN55022:2010, *CENELEC*, 2010.

[15] Lim, S.H., "Asymmetrical Duty Cycle Flyback Converter," U.S. Patent US5959850A, 28 September 1999.

[16] L. Huber and M. M. Jovanović, "Analysis, design, and performance evaluation of asymmetrical half-bridge flyback converter for universal-line-voltage-range applications," *2017 IEEE Applied Power Electronics Conference and Exposition (APEC)*, Tampa, FL, 2017, pp. 2481-2487, doi: 10.1109/APEC.2017.7931047.

[17] Han Li, Wenjun Zhou, Shiping Zhou and Xiao Yi, "Analysis and design of high frequency asymmetrical half bridge flyback converter," *2008 International Conference on Electrical Machines and Systems*, Wuhan, 2008, pp. 1902-1904.

[18] Chen T.M., Chen C.L., "Small-Signal Modeling of Asymmetrical Half Bridge Flyback Converter," in *Proc. of the CES/IEEE 5th International Power Electronics and Motion Control Conference National* Shanghai, China, 14–16 August 2006.

[19] Bhuvaneswari C. and R. S. R. Babu, "A review on LLC Resonant Converter," *2016 International Conference on Computation of Power, Energy Information and Commuincation (ICCPEIC)*, Chennai, 2016, pp. 620-623, doi: 10.1109/ICCPEIC.2016.7557268.

[20] B. Talesara, Jayapal R., Susheel B., S. N. Rao and B. K. Singh, "Efficiency enhancement of flyback converter using synchronous rectification," *2015 Annual IEEE India Conference (INDICON)*, New Delhi, 2015, pp. 1-5, doi: 10.1109/INDICON.2015.7443380.

[21] T. Yan, J. Xu, F. Zhang, J. Sha and Z. Dong, "Variable-On-Time-Controlled Critical-Conduction-Mode Flyback PFC Converter," in *IEEE Transactions on Industrial Electronics*, vol. 61, no. 11, pp. 6091-6099, Nov. 2014, doi: 10.1109/TIE.2014.2311401.

[22] C. Niou, C. Tsai and T. Chen, "A digital peak current delay compensation for primary-side regulation flyback adapter," *2018 International Symposium on VLSI Design, Automation and Test (VLSI-DAT)*, Hsinchu, 2018, pp. 1-4, doi: 10.1109/VLSI-DAT.2018.8373260.

[23] Medina-Garcia A., Schlenk M., Morales D.P., Rodriguez N., "Resonant Hybrid Flyback, a New Topology for High Density Power Adaptors," *Electronics*, vol. *7*, 363,2018, doi: 10.3390/electronics7120363.

[24] M. Kang *et al*., "Body Diode Reliability of Commercial SiC Power MOSFETs," *2019 IEEE 7th Workshop on Wide Bandgap Power Devices and Applications (WiPDA)*, Raleigh, NC, USA, 2019, pp. 416-419, doi: 10.1109/WiPDA46397.2019.8998940.

[25] D. Nardo, A. Scuto, G. Sorrentino, A. Raciti and S. A. Rizzo, "The key role of the SJ MOSFET with fast diode in high-end SMPS converters for telecom applications," *2019 AEIT International Annual Conference (AEIT)*, Florence, Italy, 2019, pp. 1-6, doi: 10.23919/AEIT.2019.8893311.

[26] J. Hong and G. Moon, "A Digitally Controlled Soft Valley Change Technique for a Flyback Converter," in *IEEE Transactions on Industrial Electronics*, vol. 62, no. 2, pp. 966-971, Feb. 2015, doi: 10.1109/TIE.2014.2352600.

[27] Medina-Garcia A., Kasper M.J. Schlenk M., Deboy G, "Asymmetrical flyback converter in high density SMPS" in *Proc. PCIM 2018*, Nuremberg, Germany, 5-7 June 2018.